Reconciling float-based and tracer-based estimates of eddy diffusivities

Andreas Klocker (aklocker@mit.edu) *

Massachusetts Institute of Technology, Cambridge, Massachusetts, USA

Raffaele Ferrari (rferrari@mit.edu)

Massachusetts Institute of Technology, Cambridge, Massachusetts, USA

Joseph H. LaCasce (j.h.lacasce@geo.uio.no)

Department of Geosciences, University of Oslo, Norway

Sophia T. Merrifield (stm@mit.edu)

Massachusetts Institute of Technology, Cambridge, Massachusetts, USA

* *Corresponding author address:* Andreas Klocker, Massachusetts Institute of Technology, 77 Massachusetts Avenue, 54-1622, Cambridge, MA 02139.

E-mail: aklocker@mit.edu

ABSTRACT

Lateral diffusivities are computed from synthetic particles and tracers advected by a velocity field derived from sea surface height measurements from the South Pacific, in a region west of Drake Passage. Three different estimates are compared: (1) the tracer-based "effective diffusivity" of Nakamura (1996), (2) the growth of the second moment of a cloud of tracer and (3) the single and two-particle Lagrangian diffusivities. The effective diffusivity measures the cross-stream component of eddy mixing, so the manuscript focusses on the meridional diffusivities for the others, as the mean flow (the ACC) is zonally-oriented in the region.

After an initial transient of a few weeks the effective diffusivity agrees well with the meridional diffusivity estimated both from the tracer cloud and from the particles. This proves that particle and tracer based estimates of eddy diffusivities are equivalent, despite recent claims to the contrary. Convergence among the three estimates requires that the Lagrangian diffusivities are estimated via their asymptotic values, not their maximum values. The former are generally much lower than the latter in the presence of a mean flow.

1. Introduction

Quantifying tracer transport by geostrophic eddies is one of the outstanding problems in large-scale ocean dynamics. Geostrophic eddies set the rate at which tracers like heat and carbon are mixed laterally and vertically in the ocean and play a central role in determining large scale circulation patterns, such as the meridional overturning circulation (see for example the reviews by Olbers et al. (2004) or Marshall and Speer (2011)).

The mixing induced by geostrophic eddies is often quantified in terms of an eddy diffusivity. The component of the diffusivity across the mean currents is most relevant, because tracer transport along currents is generally dominated by the current itself. The cross-current eddy diffusivity K is defined as,

$$\overline{v'C'} = -K\bar{C}_y, \tag{1}$$

where $\overline{v'C'}$ is the cross-current tracer flux and $\bar{C}_y$ is the cross-current tracer gradient. Overbars denote large-scale averages and primes are departures from those averages. As noted hereafter, there are discrepancies in the literature about both the magnitude and spatial patterns of K, and it is a goal of this paper to help resolve these discrepancies.

Estimates of K can be obtained from Eulerian data, from tracer distributions and from Lagrangian (particle) data. Early attempts to estimate K with Eulerian data relied on mooring time series of velocity $\boldsymbol{v}$ and tracer C (e.g. temperature) to construct $\overline{\boldsymbol{v}'C'}$ and its relationship to $\overline{C_y}$ (e.g. Bryden and Heath 1985). However, the time series are often too short for significant results (Wunsch 1999). In addition, the estimates are hampered by the presence of large, non-divergent eddy fluxes that do not contribute to mixing (Marshall and Shutts 1981).

Another example of Eulerian estimates is the use of satellite measurements of sea surface height (SSH) in conjunction with mixing length theory (Prandtl 1925) to estimate diffusivities, as proposed by Holloway (1986) and Ferrari and Nikurashin (2010). This approach has the advantage that time series at fixed locations lend themselves well to the determination of mean and residual quantities. The weakness is that the eddy diffusivity can be determined up to undetermined constants that appear in the mixing length theory.

Tracer-based estimates can be made from hydrographic data. Armi and Stommel (1983) studied the oxygen distribution in the Eastern North Atlantic in the context of an advective-diffusive equation and inferred an eddy diffusivity of approximately 500 $m^2 s^{-1}$ at 800 m depth. Similarly, Ferrari (2005) and Zika et al. (2010) used temperature and salinity observations in the same region to estimate diffusivities from $O(1000\ m^2 s^{-1})$ at the surface and $O(100\ m^2 s^{-1})$ below 1500 m. Jenkins (1998) studied tritium and ^{3}He distributions in the same region and estimated $K \sim 1200\ m^2 s^{-1}$ at a depth of 300 m.

Such estimates assume a steady state of advection and diffusion. The evolution of the eddy diffusivity can only be deduced with observations of a time-evolving tracer distribution, as in the North Atlantic Tracer Release Experiment (NATRE; Ledwell et al. (1998)). The diffusivity can then be estimated from the dispersion of the patch. The NATRE release (of sulphur hexafluoride) yielded an estimate of $K \sim 1000\ m^2 s^{-1}$ at 300 m depth, consistent with the steady-state estimates of Jenkins (1998).

Lagrangian estimates on the other hand derive from the trajectories of freely-drifting instruments, like surface drifters and subsurface floats (e.g. Davis 1991; LaCasce 2008). The diffusivity is proportional to the derivative of the mean square separation of the particles from their starting positions, as first proposed by Taylor (1921). Early diffusivity estimates from drifting buoys in the North Atlantic were made by Freeland et al. (1975), Colin de Verdiere (1983) and Krauss and Böning (1987). Colin de Verdiere (1983) obtained a meridional diffusivity of $K \sim 1700\ m^2 s^{-1}$ at the surface and Freeland et al. (1975) obtained $K \sim 700\ m^2 s^{-1}$ at 1500 m depth.

However, some subsequent estimates were much larger. Zhurbas and Oh (2004) obtained values in excess of 4000 $m^2 s^{-1}$ at the surface in the Western Atlantic, reaching values of

$20,000\ m^2s^{-1}$ in the vicinity of the Gulf Stream. Lumpkin et al. (2002) and McClean et al. (2002) found comparable values.

Diffusivities have also been measured in the Southern Ocean, which is the focus of this paper, and here too the results vary. Eulerian-based estimates, from SSH, yield values of $2000 - 4000\ m^2s^{-1}$ in the Antarctic Circumpolar Current (ACC), with smaller values in the subtropical gyres to the north (Keffer and Holloway 1988; Stammer 1998). However the tracer-based estimates differ. Using a technique proposed by Nakamura (1996) (Sec. 2), Marshall et al. (2006) obtained values of $O(1000\ m^2s^{-1})$ near the core of the ACC and *larger* values of $O(2000\ m^2s^{-1})$ to the north. This method yields only the cross-stream component of the diffusivity and thus in principle does not suffer from "contamination" by the mean flow. Lower diffusivities in the ACC are consistent with the mean flow suppressing cross-stream mixing (e.g. Ferrari and Nikurashin 2010). The ACC weakens with depth, suggesting the diffusivity should have a subsurface maximum (as the eddy field is intensified near the current). Abernathey et al. (2010) found this to be the case, using the tracer-based diagnostic.

Lagrangian estimates on the other hand tend to be larger. Lumpkin and Pazos (2007) and Sallée et al. (2008) obtained values in the vicinity of the ACC of approximately $4000\ m^2s^{-1}$, using surface drifters, with smaller values north and south of the jet. The exception was near the western boundary currents where the diffusivities were large. Consistent with some earlier studies in the North Atlantic (e.g. Lumpkin et al. (2002) and refs. therein), Sallée et al. (2008) found that K is correlated with the eddy kinetic energy; the largest values were near the ACC, where eddy variability is most pronounced. However, not all the Lagrangian estimates agree. Using synthetic float data from a numerical model, Griesel et al.

(2010) found much smaller cross-stream diffusivities ($O(750\,m^2s^{-1})$) in the polar frontal zone, consistent with the tracer-derived estimates. However, they did not observe a suppression of eddy mixing in the ACC itself, nor did their diffusivities vary with depth.

Thus there are discrepancies between the estimates particularly in the Southern Ocean. This is a significant challenge for ocean and climate simulations, because coarse-resolution models are sensitive to the magnitude and the lateral and vertical structures of eddy diffusivities in the Southern Ocean (Griffies et al. 2005; Danabasoglu and Marshall 2007). Indeed, ocean models can reproduce reasonable stratification and transports with meridional eddy diffusivities in the range of a few hundreds to one thousand m^2s^{-1} (e.g. Griffies et al. (2005)). As such, it is important to understand why the tracer, Eulerian and Lagrangian diffusivity estimates differ.

Several studies have addressed this question previously. Sundermeyer and Price (1998) used an idealized ocean model to reproduce eddy statistics from the NATRE field campaign (Ledwell et al. 1993) and simulated the motion of synthetic floats and tracers. Their Lagrangian estimates of K were 2-6 times larger than the tracer-based estimates. Riha and Eden (2011) used an idealized zonally periodic channel with eddy-driven zonal jets to compare Lagrangian and Eulerian diffusivity estimates. Interestingly, their estimates were comparable, with the Lagrangian ones being slightly smaller. Incidentally, both methods indicated an increase of the eddy diffusivities with depth.

In the present work, we examine further the relationship between different diffusivity estimates. To this end, we use a three-dimensional velocity field representative of the Southern Ocean, derived from satellite measurements of SSH, to estimate eddy diffusivities from tracers and floats. We focus on a region in the Southern Ocean upstream from Drake passage

which is the site of a large field experiment, the Diapycnal and Isopycnal Mixing Experiment in the Southern Ocean (DIMES). A major goal of DIMES is to infer eddy diffusivities from tracer and float releases. In the present paper, we focus on diffusivity estimates; in a seperate paper (Klocker et al. 2011), we examine mixing suppression by the mean flow.

The results suggest that cross-stream estimates of eddy diffusivities from both Lagrangian statistics and tracer releases converge if measured properly and if the statistics are adequate. The comparison is hindered by the mean flow, which causes the Lagrangian diffusivity to overshoot its asymptotic value. Correct estimates thus require integrating past this overshoot.

The paper is organized as follows. Section 2 examines the different methods for calculating the diffusivity and how they are related. Section 3 describes how we construct the velocity field used to advect tracers and floats and section 4 presents and compares the diffusivity esitmates for a sector of the Southern Ocean upstream of Drake Passage. The results are discussed in section 5.

2. Theory

Here we compare theoretical estimates of tracer-based and particle-based diffusivities. The former is described by Nakamura (1996), Shuckburgh and Haynes (2003) and Marshall et al. (2006). The term derives from the advection-diffusion equation for a passive tracer, $C(x, y, t)$:

$$\frac{\partial}{\partial t}C + \nabla \cdot (\boldsymbol{u}C) = \nabla \cdot (\kappa \nabla C) \tag{2}$$

where $\boldsymbol{u}$ is taken to be a 2-D (horizontal) velocity, assumed non-divergent, and κ is a small scale diffusivity. The latter might be the molecular diffusivity or a numerical diffusivity imposed to make solutions stable. The equation can be written as a simple diffusion equation when expressed in coordinates defined by the tracer isolines:

$$\frac{\partial}{\partial t}C = \frac{\partial}{\partial A}(K_{nak}\frac{\partial C}{\partial A}) \tag{3}$$

where A is the area bounded by an isoline of the tracer C, assumed to be a monotonic function of C. Further,

$$K_{nak} = \frac{\kappa}{(\partial C/\partial A)^2}\frac{\partial}{\partial A}\int |\nabla C|^2 \, dA \tag{4}$$

is Nakamura's effective diffusivity. This is proportional to the small scale diffusivity, κ, but it also depends on the gradient of C, integrated over the area bounded by the isoline. Thus if stirring acts to increase the gradients, the effective diffusivity can be much larger than the small-scale value. Note that K_{nak} has units of $(length)^4/time$, in contrast to a usual diffusivity.

Nakamura's effective diffusivity is often written in terms of a ratio of squared length scales:

$$K_e = \kappa\frac{L_{eq}^2}{L_0^2} \tag{5}$$

where L_{eq} is greater than or equal to L, the length of the tracer contour, L_0 is the initial length of the contour and $K_e = K_{nak}/L_0^2$. This form shows that the effective diffusivity exceeds the small scale value if the tracer contour is elongated by the advecting flow.

A simple way to see the preceding relation is as follows. Consider the integral of (2) over a region bounded by an isoline of tracer:

$$\iint \frac{\partial}{\partial t}C \, dA = \kappa \oint \frac{\partial C}{\partial n} \, dl = \kappa\langle\frac{\partial C}{\partial n}\rangle L \tag{6}$$

where n is the vector normal to the contour and the brackets indicate the mean value along the length of the contour. Given two tracer contours, e.g. C_1 and C_2, the mean gradient is:

$$\langle \frac{\partial C}{\partial n} \rangle = \triangle C \langle \frac{1}{\delta} \rangle \tag{7}$$

where $\triangle C = C_2 - C_1$ is the difference between the tracer values, assumed fixed, and δ is the spacing between the contours. The spacing is related to the area between the contours:

$$dA = \langle \delta \rangle L \tag{8}$$

so:

$$\langle \frac{\partial C}{\partial n} \rangle \ \geq \ \frac{\triangle C L}{dA} \tag{9}$$

because $\langle 1/\delta \rangle$ is greater than $1/\langle \delta \rangle$ as per the Cauchy-Schwarz inequality for positive-definite δ.

During the initial straining, before small scale mixing sets in, this area is approximately conserved (as the flow is non-divergent). Then the area difference, dA, can be found from the initial distribution. Assuming the contours are uniformly spaced initially, then $dA = \delta_0 L_0$. Thus:

$$\langle \frac{\partial C}{\partial n} \rangle \geq \frac{\triangle C L}{\delta_0 L_0}. \tag{10}$$

Using this, we can re-write the integrated tracer equation:

$$\iint \frac{\partial}{\partial t} C \ dA \geq K_{el} \frac{\triangle C}{\delta_0} L_0 \tag{11}$$

where K_{el} is:

$$K_{el} = \kappa \frac{L^2}{L_0^2} \tag{12}$$

Thus K_{el} is the lower bound of the effective diffusivity divided by the initial contour length squared.

We can use this to make the connection with the Lagrangian diffusivities. We think of the tracer contour as being comprised of N discrete particles. Then the squared length of the contour is given by:

$$L^2 = \sum_{n=1}^{N-1} (\boldsymbol{r}_{n+1} - \boldsymbol{r}_n)^2 = \sum_{n=1}^{N-1} (x_{n+1} - x_n)^2 + (y_{n+1} - y_n)^2 \tag{13}$$

where $\boldsymbol{r}_n = (x_n, y_n)$ is the position of the n-th particle. Clearly:

$$L^2 = N < \triangle r^2 > \tag{14}$$

where $< \triangle r^2 >$ is the mean square spacing between the particles. This is the *relative dispersion* of particle pairs (e.g. Bennett (2006)). Thus if the area between tracer isolines is conserved, we have:

$$K_{el} = \kappa \, \frac{< \triangle r^2 >}{< \triangle r_0^2 >} \tag{15}$$

So the effective diffusivity is proportional to the relative dispersion.

But how is the effective diffusivity related to the particle diffusivity? Following Taylor (1921), the Lagrangian diffusivity is given by:

$$K_1 = \frac{1}{2} \frac{d}{dt} < (\boldsymbol{r} - \boldsymbol{r}_0)^2 > \tag{16}$$

where $\boldsymbol{r}$ is the position of a particle, $\boldsymbol{r}_0$ is its initial position and the brackets indicate an average over all available particles. This applies to *single* particles, and accordingly we refer to (16) as the *single-particle diffusivity*. However, one can also define a *relative diffusivity (or two-particle diffusivity)*:

$$K_2 = \frac{1}{4} \frac{d}{dt} < \triangle r^2 > \tag{17}$$

(e.g. Batchelor and Townsend (1953); Davis (1985); Babiano et al. (1990)). The factor of

1/4 is arbitrary but useful, as described below. An important point is that the relative diffusivity, unlike the single-particle diffusivity, is Galilean invariant.

Now if the stirring is *non-local* (dominated by larger scale eddies), the relative dispersion increases exponentially in time (Lin 1972; Bennett 1984; Babiano et al. 1990; LaCasce 2008):

$$< \triangle r^2 >=< \triangle r_0^2 > \ e^{t/\tau} \tag{18}$$

where τ is a time scale, usually determined by the root mean squared shear. From (15), the effective diffusivity will also grow exponentially in time, with the same e-folding time scale, τ. With exponential growth, the relative diffusivity is proportional to the relative dispersion:

$$K_2 = \frac{1}{4\tau} < \triangle r^2 > \tag{19}$$

So the effective and relative diffusivities are proportional to one another:

$$K_{el} = \kappa \ \frac{4\tau K_2}{\langle \triangle r_0^2 \rangle} \tag{20}$$

But this equivalence follows from two assumptions: first, that the area is conserved between tracer contours and second, that the stirring is non-local. The relation will presumably break down if either assumption is violated. So, for example, the diffusivities should differ under local stirring, as occurs in a 2-D inverse energy cascade or 3-D forward energy cascade.

In numerical studies, the effective diffusivity asymptotes to a constant value when the small-scale diffusion is actively mixing away the tracer gradients (Nakamura 2008). Area is no longer conserved between isolines, implying the lower bound in (12) is no longer useful. The relative dispersion on the other hand continues to grow. When particle separations are large enough, the pair velocities are uncorrelated and the relative diffusivity, defined with the prefactor of 1/4, asymptotes to the single particle diffusivity, $K_2 \rightarrow K_1$ (e.g. Babiano

et al. (1990); LaCasce (2008)). At this point, relative dispersion grows linearly in time, as for a diffusive process. But as the effective diffusivity is constant, the two cannot be the same at later times.

The Lagrangian diffusivities (the time derivative of dispersion) should also asymptote to constant values at later times, provided there are no long-term correlations in the velocities (Taylor 1921). Yet there is no guarantee that the particle diffusivities will agree with the tracer-derived estimate. Indeed, the former derive purely from advective considerations while the latter are based on an areal integration which effectively removes the advective term from the tracer equation. While the effective diffusivity is proportional to the small-scale diffusivity, the relative diffusivity is determined essentially by the scale and kinetic energy of the energy-containing eddies. The two diffusivities are expected to converge, if the rate at which tracers are homogenized is set by the large-scale eddies and not by small scale diffusion. This likely happens in strongly turbulent fields where the large-scale eddies set the rate at which tracer filaments are generated. Once generated, the filaments are stretched and folded until they are homogenized by small scale diffusion. A reduction of small-scale diffusion does not alter the rate of tracer homogenization, rather it results in thinner filaments that can be irreversibly mixed faster to keep up with the rate of filament generation.

Previous results suggest that the two diffusivities are the same, at least for some idealized flows. A collection of particles constitutes a tracer, and thus an initial distribution should evolve according to the same diffusion equation (3). Shuckburgh and Haynes (2003) examined this, computing numerical solutions to this equation, using the effective diffusivity diagnosed from the flow field, and comparing the solutions to time-evolving distributions of particles

advected by the same flow. The close agreement suggests the particles effectively obey the same diffusion equation. So the diffusivity measured by the particles and the tracer ought to agree.

We test this hereafter using numerical calculations of evolving tracer fields and particle distributions using a velocity field representative of the surface Southern Ocean. We consider that field next.

3. The velocity field

The velocity at the surface is estimated from the sea surface height slope measured by altimeters from space. We use sea level anomaly maps from the combined processing of Ocean Topography Experiment (TOPEX) and European Remote Sensing Satellite-1 and 2 (ERS-1 and ERS-2) altimetry data with a temporal resolution of 10 days and a spatial resolution of $1/4^o$ longitude $\times$ $1/4^o$ latitude. We focus on the region upstream of Drake Passage between 103^o-78^oW and 30^o-66^oS, broadly the same area chosen for the DIMES campaign; a snapshot of sea surface height from this region is shown in Fig. 1. Conveniently, the ACC is nearly zonal in this region, so the cross-stream direction is simply north-south.

The sea level anomalies are computed with respect to a 3-year mean (from January 1993 to January 1996). The mean streamlines are computed from the sum of the mean geoid and the 3-year time-mean sea-surface height from altimetry. The geoid model is described in Lemoine (1998) and the altimetric data are described in Marshall et al. (2006) and Ferrari and Nikurashin (2010). The geostrophic relation is used to derive zonal and meridional geostrophic velocities from sea surface height slopes, $(u_g, v_g) = f^{-1}g(-\partial_y h, \partial_x h)$

where f is the Coriolis parameter and g the acceleration of gravity. The velocities are then interpolated onto a $1/10^o$ resolution grid. We constructed two different velocity fields, an 'eddy' velocity field, in which we calculate the geostrophic velocities using only the sea-surface height anomalies and a 'full' velocity field in which we add the zonal mean flow shown in Fig. 3 (ignoring the very weak meridional mean flow) to the eddy velocity. The results described below do not change if we retain the longitudinal dependence of the mean flow.

The altimeter provides an estimate for the surface horizontal velocity, but one needs horizontal velocities at all vertical levels to estimate both the horizontal and vertical variations in the lateral eddy diffusivity. Killworth and Hughes (2002) argue that the mean and eddy flows in the ACC have an equivalent-barotropic structure, i.e. the horizontal velocities at all levels can be reconstructed by multiplying the surface values by a structure function that depends only on depth, $\mu(z)$, defined as

$$\mu(z) = \frac{|\boldsymbol{u}(x, y, z)|}{|\boldsymbol{u}(x, y, 300)|}. \tag{21}$$

The equivalent-barotropic structure applies only to the geostrophic velocity, hence the velocity field is scaled to its value at $z = 300$ meters below any Ekman flow. The structure function is computed from the output of the Southern Ocean State Estimate (SOSE; Mazloff et al. 2010), an eddy-permitting general circulation model of the Southern Ocean constrained to observations in a least-squares sense. The structure function $\mu(z)$ is calculated at each vertical level as a two-year average and a spatial average restricted to the area spun by the ACC in the region under study; the equivalent-barotropic model is meant to apply only in the ACC and not north of it (Killworth and Hughes 2002). The structure function $\mu(z)$,

shown in Fig. 2, is then used to scale the surface geostrophic velocity in the whole domain (not just in the ACC latitude band) and produce a three-dimensional map of geostrophic velocity. We tested the skill of the equivalent-barotropic model in reproducing the horizontal velocity field in SOSE: the difference between the model horizontal velocity and the equivalent-barotropic model horizontal velocity is typically less than 20% in the ACC latitude band. The approach is less successful north and south of the ACC, where the error can be as large as 100%. The focus of this paper is mainly on dispersion in the ACC latitude band, so the lack of skill in reconstructing the velocity in other regions is less important. Moreover, our goal is to compare different diffusivity estimates using the same velocity field and it is not essential that the field be completely realistic.

The eddy diffusivities are computed by advecting tracers and floats along horizontal planes. All diffusivity estimates converge in less than a year, as shown below. We focus on dispersion in the meridional direction, as noted; fluid parcels experience meridional displacements of 100-200 km during the first year.

The advection of tracers and floats is purely horizontal, i.e. vertical velocities are ignored. The vertical displacements experienced in a year are less than $10 - 100\ m$. Thus the lateral dispersion is hardly affected by the additional vertical displacement. The vertical velocities are nevertheless important because they permit horizontal divergence ($\partial_x u + \partial_y v = -\partial_z w \neq 0$). Over long times fluid particles would artificially cluster in regions of convergence and drift away from regions of divergence. We therefore make the velocity field non-divergent by adding a divergent correction, $\Delta\chi$, to the altimetric velocity, i.e. we create a velocity field $\boldsymbol{u} = \boldsymbol{u}_g + \Delta\chi$, where $\boldsymbol{u}_g$ is the geostrophic velocity. The divergent correction further imposes no-normal flow conditions at the continental and north-south boundaries of the

computational domain. Periodic conditions are instead enforced at the east-west boundaries. The implementation of the non-divergent correction is described in detail in Marshall et al. (2006). In practice the adjustment leads to very small changes of the geostrophic velocity field and primarily at the boundaries. The estimates of dispersion are hardly sensitive to these corrections, except close to the meridional boundaries.

4. Methods

We now compare the effective diffusivity of Nakamura (1996) with the single-particle and two-particle diffusivities. We also estimate the diffusivity from the dispersion of tracer patches. As the effective diffusivity measures mixing across the mean flow, we focus solely on the meridional components of the diffusivities, as the mean flow in the region is primarily zonal.

We compute the effective diffusivity K_e by advecting a tracer with the equivalent-barotropic velocity field shown in Fig. 1 and using a constant numerical diffusivity κ. The approach is identical to that described in Marshall et al. (2006) and Ferrari and Nikurashin (2010) and the reader is referred to those papers for technical details. This requires careful consideration of the implicit mixing due to the numerical scheme which changes the value of κ to be used in Eq. (4) – we show in Appendix A that the implicit mixing changes with depth and these variations must be taken into account.

The meridional component of the single-particle diffusivity is defined as:

$$K_{1y}(y_0, t) = \frac{1}{2}\frac{d}{dt}\langle (y(t) - y_0)^2 \rangle, \tag{22}$$

where $y(t)$ is the meridional position of a particle released at y_0 at $t = 0$ and $\langle\cdot\rangle$ is the average over all particles. We anticipate the diffusivity will vary with latitude, so we express it as a function of the initial position, y_0.

The eddy diffusivity is equal to the integral of the Lagrangian autocorrelation function:

$$K_{1y}(y_0, t) = \int_0^t \langle R_{vv}(y_0, \tau)\rangle d\tau \qquad \text{where} \qquad R_{vv}(y_0, \tau) = \langle v_L(y_0, \tau) v_L(y_0, 0)\rangle. \tag{23}$$

Assuming that the correlation goes to zero after a given period of time and that its integral is finite, the diffusivity $K_{1y}(y_0, t)$ will asymptote to a constant value (Taylor 1921).

The relative (two-particle) diffusivity is defined analogously:

$$K_{2y}(y_0, \triangle r_0, t) = \frac{1}{4}\frac{d}{dt}\langle (y_i(t) - y_j(t))^2\rangle, \tag{24}$$

where $y_i(t)$ and $y_j(t)$ are the meridional positions of particles i and j released within a distance $\triangle r_0$ of each other (y_0 is the initial condition of either the i or j particle); the ensemble average is taken over many such pairs. As noted, we use the pre-factor of 1/4 to ensure that the two-particle diffusivity asymptotes to the single-particle value at long times (e.g. Davis (1985)).

Trajectories are generated by advecting numerical particles with the velocity field described above. The floats are initialized on a regular grid with an initial spacing of 0.2^o and advected for one year using a 4^{th}-order Runge-Kutta scheme. Float positions are saved every 0.6 days. We impose a periodic boundary condition in the zonal direction, so that floats leaving the eastern or western boundary re-enter from the opposite side. This ensures that floats do not leave the computational domain, increasing the length of the particle time series. A no-normal flow condition is imposed at the northern and southern boundaries (Sec. 3), so the floats are unable to leave there.

A few sample trajectories illustrate the different kinematic regimes in the subtropical gyre and in the ACC (Fig. 4). In the subtropical gyre, the floats have a random motion. In the ACC, on the other hand, the particles exhibit coherent, meandering motion. This meandering plays an important role in the subsequent particle statistics. Note that after 150 days many floats in the ACC would have have left the domain from the east, were they not reintroduced from the west (re-entering floats are not shown in the figure).

Lastly, there is the diffusivity derived from the dispersion of a cloud of tracer. The center second moment of the cloud is equivalent to the relative dispersion of all pairs of particles in the cloud, as long as the spreading of the tracer cloud is dominated by stirring and not by small scale diffusion (LaCasce 2008). When the pair motions become uncorrelated, the centered second moment of the cloud increases linearly in time, as for a diffusive process; at this point the diffusivity can be obtained from the time derivative of the centered second moment (Garrett 1983). The meridional component is defined:

$$K_{ty} = \frac{1}{2}\frac{\partial \sigma_y^2}{\partial t} = \frac{1}{2}\frac{\partial}{\partial t}\frac{\iint (y-y_c)^2 C(x,y)dxdy}{\iint C(x,y)dxdy}, \tag{25}$$

where σ_y^2 is the second moment of the tracer concentration in latitude and y_c is the meridional position of the baricenter of the tracer patch,

$$y_c = \frac{\iint yC(x,y)dxdy}{\iint Cdxdy} \tag{26}$$

We advected tracer patches with the same velocity field and numerical scheme described before. We used two different initial conditions: zonally uniform stripes with a meridional Gaussian profile and a standard deviation of 0.5^o latitude, and isotropic Gaussian blobs with a 0.5^o standard deviation in longitude and latitude. The zonal stripes are most appropriate

for estimating meridional diffusivities for the whole Pacific sector, while the blobs are an attempt to reproduce an anthropogenic tracer release in the real ocean.

5. Results

a. Initial behavior

We consider first the initial behavior of the effective diffusivity, and test the relation to the relative dispersion given in Eq.(15). To do this, we calculate the relative dispersion of a set of particles deployed along latitude lines and compare that to the effective diffusivity for the same latitude (technically equivalent latitude, see the Appendix).

Examples at two latitudes are shown in Fig. 5. The particle diffusivity, defined as $\kappa\langle\triangle r^2\rangle/\langle\triangle r_0^2\rangle$, is shown by the solid and dashed curves and the effective diffusivity by the dash-dot curve. The solid curve is for pairs with an initial separation of 0.1^o and the dashed curve for an initial separation of 0.02^o.

The upper panel shows the results from 45^oS, north of the ACC. The three curves track one another closely for the first 10 days and the growth is nearly exponential. Exponential growth is to be expected (e.g. Bennett (1984)), as the initial particle spacing is below the resolution of the velocity field, implying that the velocity spectrum is very steep at these scales (see also Poje et al. (2010)). After the initial period, the effective diffusivity grows slower (and saturates, soon after); the relative dispersion on the other hand continues to increase. Of these two, the dispersion with the smaller initial separation (the dashed curve) increases fastest.

The latter effect can be understood as follows. All the curves have the same initial value, equal to κ. Imagine that the exponential growth proceeds to a scale, L; this could be the deformation radius, for example. At that scale, the particle estimate of the dispersion from (12) is $\kappa L^2 / \triangle r_0^2$. So the smaller the initial spacing, the larger the diffusivity at scale L. In addition, the exponential growth is clearest with the $\triangle r_0 = 0.02^o$ spacing, as the pairs experience the interpolated velocity differences for a longer period.

The comparison at 59^oS, in the ACC latitude band, is not as good. The particle dispersion increases exponentially and the two curves with different initial separations agree with one another at early times, as before. But both grow more rapidly than the effective diffusivity. The latter asymptotes to a value near 500 $m^2 s^{-1}$ by day 25, while the particle-based estimates are much larger.

This suggests that the mean flow causes the effective diffusivity to diverge faster from the area-conserving estimate given in (12). This is due in part to the zonal dispersion of the particles by the mean flow. Rhines and Young (1983) show that tracers are rapidly homogenized along mean streamlines, so after a very short transient the tracer contours reflect only the the cross-flow diffusivity. But the relative dispersion used to evaluate L^2 also includes the zonal dispersion, and this is increasing faster due to the mean shear.

In summary, the effective diffusivity behaves like the relative dispersion of particle pairs initially. But at later times, when the effective diffusivity asymptotes, the similarity no longer holds. This is due in part to the non-conservation of area between tracer contours and because the effective diffusivity only measures the cross-flow diffusivity. Thus having a mean zonal flow worsens the agreement and it is more sensible to focus on the cross-stream

particle diffusivity at later times.

b. Asymptotic behavior; effective diffusivity

Now we turn to the diffusivities at later times. Shown in Fig. 6 is the asymptotic value of the effective diffusivity, K_e, as a function of latitude at the surface and at 1500 m. The asymptotic value is obtained by averaging the diffusivity over the period from 150-365 days, after the measure has leveled off. At the surface the eddy diffusivity is close to 1000 $m^2 s^{-1}$ north of the ACC, while it drops to 500 $m^2 s^{-1}$ in the core of the current. In contrast, the eddy diffusivity at depth is largest in the core of the ACC where it reaches 1000 $m^2 s^{-1}$ and is smaller to the north. These patterns are consistent with those of Marshall et al. (2006) and Abernathey et al. (2010).

The observed latitudinal and vertical variations in the diffusivity support the notion that the mean flow suppresses mixing (Ferrari and Nikurashin 2010). To test this, we advected the particles with a velocity field with the zonal mean flow (Fig. 3) removed: the 'eddy' velocity field introduced in Sec. 3. The resulting estimates of K_e are shown in Fig. 6. Without a mean flow, K_e peaks in the core of the ACC, where the eddy kinetic energy (EKE) is largest, both at the surface and at depth. Such behavior is consistent with mixing length arguments in which the diffusivity is proportional to the eddy length scale times the square root of the kinetic energy (Holloway 1986; Keffer and Holloway 1988). The eddy length scale varies little with depth and latitude, so that $K_e \propto \sqrt{EKE}$ as shown in Klocker et al. (2011). However, the addition of a mean flow breaks the scaling at the surface (at depth the mean flow is very weak). The suppression is more pronounced in the ACC where the mean

flow is largest. The suppression of mixing by the mean flow is the focus of a seperate paper (Klocker et al. 2011).

Fig. 7a shows the full depth-latitude map of K_e for the Pacific sector under study. In the ACC latitude band, between 55^oS and 65^oS, the diffusivity is suppressed by the mean flow at the surface and has a subsurface maximum around 1500 m where the mean flow becomes weak. To the north, where the mean flows are weaker, the diffusivity is largest at the surface where the EKE is largest.

c. Moment method: dispersion of a tracer patch

Next we consider the diffusivities as estimated from the growth of a patch of tracer. Fig. 6 shows the eddy diffusivity for a series of zonal "stripes" of tracer, released at different latitudes at the surface and at 1500 m. The growth rate of σ_y^2 becomes linear in time after 150 days. We estimate the eddy diffusivity K_{ty} as a least square fit of the change in σ_y^2 versus time between 150 and 365 days. The K_{ty} estimated from Eq. (25) agree well with the effective diffusivities K_e at all latitudes, despite some discrepancies at the northern and southern boundaries where edge effects suppress the dispersion.

Results from the Gaussian patch releases are also shown in Fig. 6. Patches were released at 100^oW at different latitudes, at the surface and at 1500 m. The initial transient is much more variable in these simulations, but after 150 days the dispersion is increasing linearly, allowing the eddy diffusivity to be computed over the interval from 150 - 365 days. Agreement with the previous estimates is very good. Again discrepancies are visible at the north and south edges of the domain, and also between $53^o - 54^o$S. The latter is the result of the rapid

zonal variations in eddy diffusivity at the northern edge of the ACC.

Note that while the effective diffusivity and the zonal stripes yield a zonal average of the eddy diffusivity, the Gaussian patches at early times can be used to detect longitudinal variations. Averaging the results from patches released across the domain in the zonal direction yields the same diffusivity as with the stripe (not shown here). Note that agreement between different methods is achieved because we can sample all of the tracer (periodic boundary conditions ensure that the tracer never leaves the domain). Such sampling cannot be done in field experiments.

d. Particle dispersion

Lastly, we consider diffusivities derived from particle trajectories. We begin with the single-particle diffusivity, as this is the measure used most frequently in observational studies. We calculated $K_{1y}(y_0, t)$ using Eq. (22)—estimating the diffusivity by integrating the velocity autocorrelation yielded identical results. We averaged the diffusivities for all particles deployed in regions 25^o in longitude (the width of the domain) by 2^o in latitude. This bin size is substantially larger than the typical eddy scale in the Southern Ocean of $O(100)$ km. As the mean velocity is purely zonal, we do not need to separate mean and eddy velocities in the meridional direction.

Following Davis (1991), we treat every point at which a float position is saved as a starting position for a new trajectory, substantially increasing the number of pseudo-trajectories. The method is illustrated graphically in Fig. 8: every orange dot shows a point at which a float position is saved and it is treated as the starting position for a new trajectory. Both forward

and backward trajectories are used. The technique is described by Griesel et al. (2010) and represents a slight modification of the technique used in Colin de Verdiere (1983) and Poulain and Niiler (1989). The single-particle eddy diffusivities converge to a constant within half a year in the subtropical gyres and sooner elsewhere. Hence we consider all trajectories with a minimum length of 160 days and estimate the diffusivity as an average over the last 20 days of all available pseudo-trajectories. The averaging window is different from tracer-based estimates because particles drift too far from their release latitude after 160 days to allow local in latitude estimates of diffusivities.

Examples of single-particle diffusivities are shown in Fig. 9 for (a) particles released in a 2^o bin in the subtropical gyre ($45^oS \pm 1^o$) and (b) particles released in a 2^o bin in the ACC ($59^oS \pm 1^o$). In line with the previous calculations of effective diffusivity, we use both the full velocity field (solid lines) and the eddy velocity field (dashed lines). These bins were chosen because they are representative of regions with (a) weak mean flow and (b) strong mean flow (see Fig. 4 for the different behavior of trajectories in these regions). The shaded areas around the single-particle diffusivities show the 2σ errors estimated using a bootstrapping technique.[1] For comparison, the corresponding Lagrangian autocorrelation functions, R_{vv}, are shown in Fig. 10.

In the northern-most domain, the diffusivities based on particles advected by the eddy velocity field asymptote to a constant value of $\backsimeq 2000\ m^2 s^{-1}$ after 20 days (Fig. 9a). The

[1]Bootstrapping consists of first sub-sampling the approximately 1000 floats deployed in every bin 100 times, allowing for duplicates, and then using each of these subsets of floats to calculate a diffusivity. The 2σ errors are the standard deviations of the Ks estimated from the 100 realizations. This is the same approach to calculate confidence intervals used by Griesel et al. (2010).

diffusivity for the particles advected with the full velocity behaves similarly initially, but only reaches a value of $\backsimeq 1700\ m^2 s^{-1}$; thereafter it decreases slowly. This decrease is related to a negative lobe in the velocity autocorrelation, R_{vv} (Fig. 10a).

The difference between the diffusivities based on the eddy and mean velocity fields is more evident in the southern domain (Fig. 9b). The velocity autocorrelations for the experiments with and without a mean flow have negative lobes, but the addition of a mean flow results in a much more pronounced lobe. As a result, both diffusivities decrease after first reaching a maximum, at roughly 4000 $m^2 s^{-1}$. But, the diffusivity for the mean velocity falls much more, eventually asymptoting to a value between 500-1000 $m^2 s^{-1}$. The diffusivity for the eddy velocity is 2-3 times larger. The difference is again linked to a negative lobe in the autocorrelation, which is most pronounced with the mean flow.

The link between mean flows and negative lobes is explained in detail in a seperate paper (Klocker et al. 2011), but it can be easily understood. The mean flow in the ACC is directed eastward flowing at $10\ cm\ s^{-1}$, while the eddies drift much slower at $1-2\ cm\ s^{-1}$. Hence the mean flows advects particles around nearly stationary eddies, resulting in back and forth meandering motions. The negative lobe in the velocity autocorrelation is the signature of trajectories that meander back and forth from their release latitude. These meanders do not contribute any irreversible mixing and must not be included in the calculation of the diffusivity. This is achieved by integrating the velocity autocorrelation past the negative lobe.

Now we use Eq. (22) to compute meridional profiles of eddy diffusivities for velocities at the surface and at 1500 m depth. We employ the 25^o longitude $\times$ 2^o latitude bins described above, but with one bin every 1^o of latitude (i.e. the bins overlap). Again, the deep velocity

field is obtained by multiplying the surface velocity by the equivalent-barotropic structure function $\mu(1500\ m)$ (see Fig. 2).

The results are plotted in Fig. 11, along with the effective diffusivities found previously. The estimates agree within the errors at all latitudes, at both depths. Both estimates capture the suppression by the strong ACC flow at the surface. We therefore can answer positively to the question we posed in the introduction. For the flow regimes observed in the Southern Ocean, estimates of eddy diffusivity based on tracers and particles are equivalent. This is very encouraging, because numerical models need the eddy diffusivity that describes the rate at which tracers are homogenized, while direct estimates of diffusivity in the ocean rely on float dispersion (especially below the surface). Agreement between the two estimates means that we can compare models and observations.

In a number of previous studies, the single-particle diffusivity was estimated either from the maximum value achieved by K_{1y} at short times or, equivalently, by integrating to the first zero crossing of the velocity autocorrelation (e.g. Freeland et al. 1975; Poulain and Niiler 1989). The reasoning is that the error in the diffusivity grows in time, so that the estimates at longer lags are less certain. Alternatively some studies fit the velocity autocorrelation with an exponential curve and estimate the asymptotic value from that (e.g. Garraffo et al. 2001; Sallée et al. 2008). Both methods depend on the initial behavior of the diffusivity and miss the contribution from the negative lobe.

Integrating our velocity autocorrelations to the first zero crossing yields much larger diffusivities (not shown). Moreover, there was little difference between the diffusivities found using the full velocity and the eddy velocity. Thus using the first zero crossing method effectively eliminates the suppression of eddy diffusivity by the mean flow.

How many particles are required to obtain convergent estimates, i.e. to fully resolve the negative lobes? In the calculations above, we used approximately 1000 floats per bin, a quantity which is unrealistic by observational standards. From theory (e.g.Davis (1991)), the error in the diffusivity is expected to decrease as $n^{-1/2}$. We checked this by recalculating the diffusivities using smaller numbers of particles, both for particles released in 2^o bins in the subtropical gyre ($45^oS \pm 1^o$) and for particles released in 2^o bins in the ACC ($45^oS \pm 1^o$). Errors were calculated by the same bootstrapping technique used for Fig. 9. The relative errors defined as $2\sigma/K_{1y}$ are shown in Fig. 12, where σ is the standard deviation calculated from bootstrapping, plotted against the number of particles used. The results are consistent with a decrease proportional to $n^{-1/2}$ (although the decrease is somewhat faster with large numbers of particles). Thus the errors for realistic deployments decrease less than linearly with the number of particles with daunting implications for observational programs as discussed in the next section.

Lastly, we consider the diffusivities derived from pairs of particles. These are calculated as with the single-particle diffusivities, but now at every point at which a float trajectory is saved we find all other trajectories which are within a specified radius. We then calculate two-particle diffusivities using the meridional distance between those floats according to Eq. (24). This method thus involves using "chance pairs", or pairs of particles not deployed together (Morel and Larcheveque 1974; LaCasce 2008). We use particle trajectories with a minimum length of 60 days and average over the last 20 days. The resulting two-particle diffusivities, together with the single-particle diffusivities from the same bin, are shown in Fig. 13.

As noted previously, the two-particle diffusivity (defined with a pre-factor of 1/4) should

asymptote to the single-particle diffusivity after the pair velocities become decorrelated. This is the case (Fig. 13). However, the two-particle diffusivity differs at early times. This can be seen in Fig. 14 in which we changed the initial spacing of the particle pairs between 0.2^o and 0.8^o. At 45^oS (Fig. 14a), the closer the initial pairs, the more slowly the diffusivity asymptotes to the final value. This is because it takes longer for pairs to separate to a distance at which their motion is no longer correlated. The effect is more dramatic at 59^oS where there is a stron mean flow (Fig. 14b); we see that the overshoot is greatly diminished for closer pairs. For the smallest initial separation of 0.2^o, there is barely any overshoot at all.

The lack of overshoot in K_{2y} is that relative dispersion, unlike single-particle dispersion, is Gallilean invariant. Thus a pair of particles moves with the meandering flow (Fig. 7), and the diffusivity measures only their separation. The closer the particles are initially, the more faithfully they track one another through the meanders.

The pair diffusivities as a function of latitude are shown in red in Fig. 11. We see that the estimates are consistent with both those from single particles and with the effective diffusivities. Thus all three methods yield consistent values.

6. Summary and discussion

We have calculated lateral diffusivities for synthetic particles advected with a proxy velocity field. The latter derives from sea surface height measurements from the South Pacific, in a region west of Drake Passage. The geostrophic surface velocities were adjusted to yield a non-divergent field, and the velocities were projected downward in the water

column assuming an equivalent-barotropic structure.

We calculated the diffusivities in three ways: 1) by using a tracer to estimate the "effective diffusivity" (Nakamura 1996), 2) from the second moment of the tracer distribution and 3) via single and two-particle diffusivities. The effective diffusivity measures the cross-stream component, so we focused on the meridional diffusivities for the others, as the mean flow (the ACC) is zonally-oriented in the region.

We show that the effective diffusivity at early times is proportional to the relative dispersion (between pairs of particles). At later times, the relation breaks down as small scale mixing violates area conservation between tracer isolines. However, at the later times the effective diffusivity agrees well with the meridional diffusivity estimated both from the tracer cloud and from the particles. While our analysis focussed on the Southern Ocean, the agreement is expected to hold in other parts of the world's oceans.

The effective diffusivity is most useful for satellite-derived velocity fields, such as this, or for model fields; it is probably not practical with *in situ* tracer deployments. The moment method has been used previously with deployed tracer (e.g. Sundermeyer and Price (1998)), but obtaining sufficient sampling is also an issue. Thus float/drifter based studies are still the most desirable. The present results demonstrate that the float-derived estimates are consistent with the others, as long as they are calculated correctly.

A critical issue, seen clearly here, is that a mean flow suppresses the cross-stream diffusivities (e.g. Ferrari and Nikurashin (2010); Naveira Garabato et al. (2011)). One finds that the particle-based diffusivity reaches a maximum value before decreasing to a lower asymptotic limit. This reduction, often seen in observations, reflects a negative lobe in the velocity autocorrelation. Physically, this corresponds to "meandering" motion — particles

being advected first across the mean flow and then returning some distance back toward their starting location. Thus the initial maximum is a transient advective feature, and does not reflect the true mixing. Indeed, a similar overshoot is not seen with the effective diffusivity. Given this, using the maximum diffusivity, or equivalently integrating the autocorrelation to the first zero crossing, yields artificially large diffusivities.

There are two ways around this. One is to average the diffusivity after the initial transient phase, i.e. after it has reached the lower asymptotic limit. This means choosing an "intermediate" averaging period, after the initial transient but before the measurement errors have grown too large (e.g. Koszalka and LaCasce (2010)). The second is to use the two-particle diffusivity, which relates to the separation between pairs of particles. As both particles in the pair experience the initial meander, the relative diffusivity is devoid of the initial maximum provided the initial pair separation is small enough. However, this requires having a sufficient number of pairs to obtain reliable statistics.

A motivation for the present work was to see how many floats are required to distinguish lateral and vertical variations in eddy diffusivities in the real ocean. This is a relevant point for field campaigns such as the Diapycnal and Isopycnal Mixing Experiment in the Southern Ocean (DIMES). In DIMES, both floats and an anthropogenic tracer have been released to infer eddy diffusivities. The tracer was released at 58^oS/107^oW between the Polar Front and the Subantarctic Front on the 27.9 $kg\ m^{-3}$ neutral density surface, which is at a depth of approx. 1500 m (see Ledwell et al. (2011) for details on the tracer release). Due to the filamentation and the sparse sampling of the tracer in time (i.e. every 6-12 months) and in space (i.e. only part of the tracer is found using shipboard CTDs due to coarse sampling), it is impossible to calculate eddy diffusivities from the tracer using the methods described

above. In addition to the tracer, 150 isopycnal RAFOS floats have been released between 54^oS-60^oS/105^oW on two isopycnal surfaces: 100 on the same neutral density surface as the tracer and the other 50 on the 27.2 $kg\ m^{-3}$ neutral density surface (at a depth of approx. 500 m). These two density surfaces were chosen to see if eddy mixing is indeed suppressed in the shallow ACC relative to eddy diffusivities at mid-depth, as found in our study (e.g. Fig. 7).

To estimate the number of floats necessary to assess this vertical variation in the real ocean, we advect synthetic floats using the same velocity field as above, with the only difference that floats exiting the domain are not allowed to reenter (in the case of DIMES these floats are lost past Drake passage). The velocity field for both surfaces is derived by scaling the surface geostrophic velocity field according to the equivalent-barotopic scale factors shown in Fig. 2 (i.e. $\mu(500\ m) \sim 0.9$ and $\mu(1500\ m) \sim 0.4$). The diffusivities are computed for a bin in the ACC, which extends from 54^o to 62^oS, and a bin north of the ACC, which extends from 42^o to 50^oS - both bins span the whole domain in longitude. These bins are larger than the bins used above to increase the Lagrangian statistics per bin as needs to be done in real experiments. We consider a bin to the north to the ACC, even though no floats in DIMES were released in this region, to see if one can distinguish the eddy diffusivities in the ACC and to the north using float numbers like those in DIMES. On both surfaces floats are initialized every 0.2^o as for previous calculations, giving approximately 5000 floats per bin. The error bars are the 5th and 95th-percentiles calculated using a bootstrapping technique with 100 subsamples. We use subsample sizes of (a) 50 floats, (b) 150 floats and (c) 1000 floats. The error estimates are shown as gray shaded areas in Fig. 15.

The error bars in Fig. 15 show that with 50 or 150 floats, it is not possible to detect

differences in the eddy diffusivities between the two latitudes/depth levels with any significance. That is, we cannot resolve the lateral and vertical variations of the diffusivities in the DIMES region. With 1000 floats however, one can resolve with statistical significance the latitudinal and vertical variations in the diffusivity. This suggests that the 150 floats deployed in DIMES are not sufficient to resolve the lateral and vertical variations, if they are present. In addition note that the DIMES floats are not deployed homogeneously as in our calculations. Hence the errors shown here are a lower limit for the errors expected from float releases in DIMES.

We conclude that large errors in float-based estimates of diffusivities are endemic to field campaigns, like DIMES, because it is not conceivable to deploy $O(1000)$ floats. Thus float-derived estimates should be used in conjunction with other information to quantify the absolute values and the vertical and lateral structure of eddy diffusivities. This could come from the release of a tracer patch, such as in DIMES, satellite-derived geostrophic velocity fields, high-resolution numerical models and from theoretical models. The challenge for the future is to learn how to combine such diverse data sets to obtain statistically robust estimates of diffusivities.

Acknowledgments.

This work was done as part of the Diapycnal and Isopycnal Mixing Experiment in the Southern Ocean (DIMES). We wish to acknowledge the generous support of NSF through awards OCE-0825376 (RF and AK) and OCE-0849233 (SM). We also wish to thank all the DIMES principal investigators for many useful discussions and suggestions.

APPENDIX

To advect a numerical tracer, we use the offline capabilities of the Massachusetts Institute of Technology general circulation model (MITgcm, Marshall et al. (1997)) with the non-divergent velocity field described above and solve the tracer advection-diffusion equation

$$\frac{\partial}{\partial t}C + \boldsymbol{u} \cdot \nabla C = \kappa \nabla^2 C, \tag{A1}$$

where C is the tracer concentration and κ is the explicit numerical diffusivity. For the tracer advection we use an Adams-Bashforth time-stepping scheme and a centered 2^{nd} order advection scheme to advect the tracer for one year. The domain is zonally periodic with no-flux boundary conditions imposed at the northern and southern boundaries. The initial tracer concentration increases linearly with latitude, with values of zero at the southern boundary and values of one at the northern boundaries. As shown by Shuckburgh et al. (2009) the calculations of effective diffusivities are not very sensitive to the tracer initial condition.

The most problematic part in calculating effective diffusivities is the total numerical diffusivity. For an artificial tracer advected by a numerical model this is the sum of the explicit and implicit numerical diffusivities. Without knowing the total numerical diffusivity, but assuming that it is constant, one can determine the spatial structure of K_e, but to compute magnitudes of effective diffusivities one needs an estimate of the total numerical diffusivity (Shuckburgh et al. 2009). Marshall et al. (2006) show that the estimate of K_e becomes independent of numerical diffusivity only for large Péclet number, with $Pe = UL_{eddy}/\kappa_{total}$, where U is the characteristic scale of the velocity and L_{eddy} is an eddy length scale, and κ_{total} is the total numerical diffusivity. This would suggest to use a small κ for our calcula-

tions. On the other hand using a κ which is too small introduces implicit numerical diffusion generated by noise on the grid scale which acts to increase κ_{total}. For every vertical level we choose an explicit numerical diffusivity small enough to ensure that the estimate of K_e is independent of the numerical diffusivity, but large enough to keep the implicit numerical diffusivity small. To estimate the total numerical diffusivity inherent in the advection of the artificial tracer we use the tracer variance equation,

$$\frac{1}{2}\frac{\partial\langle C^2\rangle}{\partial t} = -\kappa\langle|\nabla C|^2\rangle, \tag{A2}$$

where $\langle\cdot\rangle$ indicates the average over the domain. κ_{total} is the total numerical diffusivity necessary to explain the decay of the observed tracer variance $\langle C^2\rangle$.

K_e is estimated by advecting the tracer with an explicit numerical diffusivity of 10 m^2s^{-1}. Using Eq.(A2) gives us the numerical background diffusivity inherent in the numerical advection code, κ_{total}, which varies from 30 m^2s^{-1} at the surface to 11 m^2s^{-1} at depth. Note that this variation of κ_{total} with depth can easily be accounted for in the two-dimensional calculations performed in this study but might lead to serious issues in three-dimensional calculations in which one value for κ_{total} is used everywhere.

We then use Eq.(5) to calculate K_e, where $L_0(y_{eq})$ is the width of the domain at the equivalent latitude y_{eq} and L^2_{eq} can be written as (see Shuckburgh and Haynes (2003) for a derivation).

$$L^2_{eq} = \left[\frac{1}{(\frac{\partial C}{\partial A})}\frac{\partial}{\partial A}\int_A |\nabla C| dA\right]^2, \tag{A3}$$

where C is the tracer concentration and A is the area between tracer contours.

REFERENCES

Abernathey, R., J. Marshall, M. Mazloff, and E. Shuckburgh, 2010: Critical layer enhancement of mesoscale eddy stirring in the Southern Ocean. *Journal of Physical Oceanography*, **40**, 170–184.

Armi, L. and H. Stommel, 1983: Four views of a portion of the North Atlantic subtropical gyre. *Journal of Physical Oceanography*, **13**, 828–857.

Babiano, A., C. Basdevant, P. LeRoy, and R. Sadourny, 1990: Relative dispersion in two-dimensional turbulence. *Journal of Fluid Mechanics*, **214**, 535–557.

Batchelor, G. K. and A. A. Townsend, 1953: Turbulent diffusion. *Surveys in Mechanics*, **23**, 352–398.

Bennett, A. F., 1984: Relative dispersion: local and nonlocal dynamics. *Journal of Atmospheric Sciences*, **41**, 1881–1886.

Bennett, A. F., 2006: *Lagrangian Fluid Dynamics*. Monographs on Mechanics, Cambridge University Press, Cambridge, 286 pp, ISBN-10: 0521853109.

Bryden, H. L. and R. A. Heath, 1985: Energetic eddies at the northern edge of the Antarctic Circumpolar Current. *Progress in Oceanography*, **14**, 65–87.

Colin de Verdiere, A., 1983: Lagrangian eddy statistics from surface drifters in the eastern North Atlantic. *Journal of Marine Research*, **41**, 375–398.

642 Danabasoglu, G. and J. Marshall, 2007: Effects of vertical variations of thickness diffusivity
643 in an ocean general circulation model. *Ocean Modelling*, **18**, 122–141.

644 Davis, R., 1985: Drifter observations of coastal surface currents during CODE: the statistical
645 and dynamical view. *Journal of Geophysical Research*, **90**, 4756–4772.

646 Davis, R., 1991: Observing the general circulation with floats. *Deep-Sea Research*, **38A**,
647 S531–S571.

648 Ferrari, K. L., R. Polzin, 2005: Finescale structure of the t-s relation in the eastern North
649 Atlantic. *Journal of Physical Oceanography*, **35**, 1437–1454.

650 Ferrari, R. and M. Nikurashin, 2010: Suppression of eddy diffusivity across jets in the
651 Southern Ocean. *Journal of Physical Oceanography*, **40**, 1501–1519.

652 Freeland, H., P. Rhines, and T. Rossby, 1975: Statistical observations of the trajectories of
653 neutrally buoyant floats in the North Atlantic. *Journal of Marine Research*, **33**, 383–404.

654 Garraffo, Z., A. Mariano, A. Griffa, and C. Veneziani, 2001: Lagrangian data in a high-
655 resolution numerical simulation of the North Atlantic. I. Comparison with in-situ drifter
656 data. *Journal of Marine Systems*, **29**, 157–176.

657 Garrett, C., 1983: On the initial streakiness of a dispersion tracer in two- and three-
658 dimensional turbulence. *Dynamics of Atmospheres and Oceans*, **7**, 265–277.

659 Griesel, A., S. T. Gille, J. Sprintall, L. McClean, J, H. LaCasce, J, and M. E. Maltrud, 2010:
660 Isopycnal diffusivities in the Antarctic Circumpolar Current inferred from Lagrangian
661 floats in an eddying model. *Journal of Marine Research*, **66**, 441–463.

662 Griffies, S. M., et al., 2005: Formulation of an ocean model for global climate simulations.
663 *Ocean Science*, **1**, 45–79.

664 Holloway, G., 1986: Estimation of oceanic eddy transports from satellite altimetry. *Nature*,
665 **323**, 243–244.

666 Jenkins, W. J., 1998: Studying subtropical thermocline ventilation and circulation using
667 tritium and ^{3}He. *Journal of Geophysical Research*, **103**, 15 187–15 831.

668 Keffer, T. and G. Holloway, 1988: Estimating Southern Ocean eddy flux of heat and salt
669 from satellite altimetry. *Nature*, **332**, 624–626.

670 Killworth, P. D. and C. W. Hughes, 2002: The Antarctic Circumpolar Current as a free
671 equivalent-barotropic jet. *Journal of Marine Research*, **60**, 19–45.

672 Klocker, A., R. Ferrari, and J. H. LaCasce, 2011: Estimating suppression of eddy mixing by
673 mean flows, Journal of Physical Oceanography, submitted.

674 Koszalka, I. and J. H. LaCasce, 2010: Lagrangian analysis by clustering. *Ocean Dynamics*,
675 **60**, 957–972.

676 Krauss, W. and Böning, 1987: Lagrangian properties of eddy fields in the northern North
677 Atlantic as deduced from satellite-tracked buoys. *Journal of Marine Research*, **45**, 259–
678 291.

679 LaCasce, J. H., 2008: Statistics from Lagrangian observations. *Progress in Oceanography*,
680 **77**, 1–29.

Ledwell, J. R., L. C. St. Laurent, J. B. Girton, and J. M. Toole, 2011: Diapycnal mixing in the Antarctic Circumpolar Current. *Journal of Physical Oceanography*, **41**, 241–246.

Ledwell, J. R., A. J. Watson, and C. S. Law, 1993: Evidence for slow mixing across the pycnocline from an open-ocean tracer-release experiment. *Nature*, **365**, 701–703.

Ledwell, J. R., A. J. Watson, and C. S. Law, 1998: Mixing of a tracer in a pycnocline. *Journal of Geophysical Research*, **103**, 21 499–21 529.

Lemoine, F. e. a., 1998: *The development of the NASA GSFC and NIMA joint geophysical model*. Tokyo, Japan, IAG, Proc. Int. Symp. on Gravity.

Lin, J.-T., 1972: Relative dispersion in the enstrophy-cascading inertial range of homogeneous two-dimensional turbulence. *Journal of Atmospheric Sciences*, **29**, 394–395.

Lumpkin, R. and M. Pazos, 2007: Measuring surface currents with surface velocity program drifters: The instruments, its data and some recent results. *Lagrangian Analysis and Prediction of Coastal and Ocean Dynamics*, A. e. a. Griffa, Ed., Cambridge University Press, 39–67.

Lumpkin, R., A.-M. Treguier, and K. Speer, 2002: Lagrangian Eddy Scales in the Northern Atlantic Ocean. *Journal of Physical Oceanography*, **32**, 2425–2440.

Marshall, J., A. Adcroft, C. Hill, L. Perelman, and C. Heisey, 1997: A finite-volume, incompressible Navier Stokes model for studies of the ocean on parallel computers. *Journal of Geophysical Research*, **102**, 5753–5766.

Marshall, J., E. Shuckburgh, J. H., and C. Hill, 2006: Estimates and implications of surface

701 eddy diffusivity in the Southern Ocean derived from tracer transport. *Journal of Physical*
702 *Oceanography*, **36**, 1806–1821.

703 Marshall, J. and G. J. Shutts, 1981: A note on rotational and divergent eddy fluxes. *Journal*
704 *of Physical Oceanography*, **11**, 1677–1680.

705 Marshall, J. and K. Speer, 2011: Closing the meridional overturning circulation through
706 Southern Ocean upwelling, Nature Geoscience, in press.

707 Mazloff, M. R., P. Heimbach, and C. Wunsch, 2010: An eddy-permitting Southern Ocean
708 state estimate. *Journal of Physical Oceanography*, **40**, 880–899.

709 McClean, J. L., P.-M. Poulain, J. W. Pelton, and M. E. Maltrud, 2002: Eulerian and
710 Lagrangian statistics from surface drifters and a high-resolution pop simulation in the
711 North Atlantic. *Journal of Physical Oceanography*, **32**, 2472–2491.

712 Morel, P. and M. Larcheveque, 1974: Relative dispersion of constant-level balloons in the
713 200 mb general circulation. *Journal of Atmospheric Sciences*, **31**, 2189–2196.

714 Nakamura, N., 1996: Two-dimensional mixing, edge formation, and permeability diagnosed
715 in area coordinates. *Journal of Atmospheric Science*, **53**, 1524–1537.

716 Nakamura, N., 2008: Quantifying inhomogeneous, instantaneous, irreversible transport using
717 passive tracer as a coordinate. *Transport and Mixing in Geophysical Flows, Lecture Notes*
718 *in Physics 744*, J. B. Weiss and A. Provenzale, Eds., Springer-Verlag Berlin Heidelberg,
719 137–164, iSBN:978-3-540-75214-1.

720 Naveira Garabato, A. C., R. Ferrari, and K. L. Polzin, 2011: Eddy stirring in the Southern
721 Ocean, Journal of Geophysical Research, in press.

722 Olbers, D., D. Borowski, C. V. lker, and J.-O. Wolff, 2004: The dynamical balance, transport
723 and circulation of the Antarctic Circumpolar Current. *Antarctic Science*, **16**, 439–470.

724 Poje, A. C., A. C. Haza, T. M. Özgökmen, M. G. Magaldi, and Z. D. Garraffo, 2010:
725 Resolution dependent relative dispersion statistics in a hierarchy of ocean models. *Ocean*
726 *Modelling*, **31**, 36–50.

727 Poulain, P.-M. and P. P. Niiler, 1989: Statistical analysis of the surface circulation in the
728 california current system using satellite-tracked drifters. *Journal of Physical Oceanography*,
729 **19**, 1588–1603.

730 Prandtl, L., 1925: Bericht über Untersuchungen zur ausgebildeten Turbulenz. *Z. Angew.*
731 *Math. Mech.*, **5**, 136–139.

732 Rhines, P. W. and W. R. Young, 1983: How rapidly is a passive scalar mixed within closed
733 streamlines? *Journal of Fluid Mechanics*, **133**, 133–145.

734 Riha, S. and C. Eden, 2011: Lagrangian and eulerian lateral diffusivities in zonal jets, Ocean
735 Modelling, in press.

736 Sallée, J. B., K. Speer, R. Morrow, and R. Lumpkin, 2008: An estimate of Lagrangian
737 eddy statistics and diffusion in the mixed layer of the Southern Ocean. *Journal of Marine*
738 *Research*, **66**, 441–463.

739 Shuckburgh, E. and P. Haynes, 2003: Diagnosing transport and mixing using a tracer-based
740 coordinate system. *Physics of Fluids*, **15**, doi:10.1063/1.1610 471.

741 Shuckburgh, E., H. Jones, J. Marshall, and C. Hill, 2009: Robustness of an effective diffusivty
742 diagnostic in oceanic flows. *Journal of Physical Oceanography*, **39**, 1992–2009.

743 Stammer, D., 1998: On eddy characteristics, eddy transports, and mean flow properties.
744 *Journal of Physical Oceanography*, **28**, 727–739.

745 Sundermeyer, M. A. and J. F. Price, 1998: Lateral mixing and the North Atlantic Tracer
746 Release Experiment: Observations and numerical simulations of Lagrangian particles and
747 a passive tracer. *Journal of Geophysical Research*, **103**, 21 481–21 497.

748 Taylor, G. I., 1921: Diffusion by continuous movements. *Proc. London Math. Soc.*, **20**, 196–
749 211.

750 Wunsch, C., 1999: Where do ocean eddy heat fluxes matter? *Journal of Geophysical Re-*
751 *search*, **104**, 13 235–13 249.

752 Zhurbas, V. and I. S. Oh, 2004: Drifter-derived maps of lateral diffusivity in the Pacific
753 and Atlantic Oceans in relation to surface circulation patterns. *Journal of Geophysical*
754 *Research*, **109**, doi:10.1029/2003JC002 241.

755 Zika, J. D., T. J. McDougall, and B. M. Sloyan, 2010: Weak mixing in the eastern North At-
756 lantic: An application of the tracer-contour inverse method. *Journal of Physical Oceanog-*
757 *raphy*, **40**, 1881–1893.

List of Figures

779 6 The effective diffusivity K_e (solid blue lines) defined in Eq. (5), the tracer-
780 based diffusivity K_{ty} defined in Eq. (25) from the spreading of tracer stripes
781 (solid black lines) and tracer patches (solid red lines). Also shown is the
782 effective diffusivity for a tracer advected with the eddy velocity only (dashed
783 blue lines). (a) Diffusivities computed with the surface geostrophic velocity
784 field. (b) Diffusivities calculated with the equivalent-barotropic velocity field
785 rescaled for $\sim 1500\ m$. 50

786 7 Latitude-depth maps of (a) the effective diffusivity K_e (Eq. (5)) and (b) the
787 single-particle diffusivity K_{1y} (Eq. (22)) $[m^2 s^{-1}]$. Eddy diffusivities were cal-
788 culated at 10 depth levels, using the equivalent-barotropic velocity field de-
789 scribed in Sec. 3. 51

790 8 The rectangular box sketches a bin sample used for calculating particle diffu-
791 sivities from two example trajectories. The orange dots are points at which
792 the trajectory positions are saved. Absolute/relative dispersion are calculated
793 using each of these points as a deployment location, i.e. each of these points
794 is the start of a pseudotrajectory. 52

795 9 The single-particle diffusivity, K_{1y} (Eq. (22)) for particles released in 2^o bins
796 in (a) the subtropical gyre ($45^o S \pm 1^o$) and (b) in the ACC ($59^o S \pm 1^o$), both
797 for the full velocity field (solid lines) and for the eddy velocity field (dashed
798 lines). The shaded error bars show 2σ errors estimated by a bootstrapping
799 technique. 53

10 The Lagrangian velocity autocorrelations, R_{vv}, corresponding to the diffusivities shown in Fig.9, for (a) particles released in a 2^o bin in the subtropical gyre ($45^oS \pm 1^o$) and (b) particles released in a 2^o bin in the ACC ($59^oS \pm 1^o$), both for the full velocity field (solid lines) and the eddy velocity field (dashed lines). 54

11 The effective diffusivity K_e (blue lines) as defined in Eq. (5), the single-particle diffusivity K_{1y} (solid black line) as defined in Eq. (22) and the two-particle diffusivity K_{2y} as defined in Eq. (24) for tracers and particles advected with (a) the surface geostrophic velocity and (b) the velocity at $\sim$ 1500 m, i.e. the surface geostrophic velocity multiplied by 0.4 according to the equivalent-barotropic model for that depth (see Fig. 2). The dashed blue lines are the effective diffusivity K_e for a tracer advected with the eddy velocity only. 55

12 Relative error $2\sigma/K_{1y}$ of the single-particle diffusivity K_{1y} (Eq. (22)), where σ is the standard deviation calculated from bootstrapping with 100 sub-samples of n particles. The errors are shown for particles released in a 2^o bin in the subtropical gyre ($45^oS \pm 1^o$) (blue) and particles released in a 2^o bin in the ACC ($59^oS \pm 1^o$) (red) for the surface (solid lines) and deep surface (dashed lines). The solid black line shows a line with slope of $n^{-1/2}$. 56

13 The time evolution of the single-particle diffusivities K_{1y} (Eq. (22), solid line) and the relative diffusivities K_{2y} (Eq. (24), dashed line) for (a) particles released in a 2^o bin in the subtropical gyre ($45^oS \pm 1^o$) and (b) particles released in a 2^o bin in the ACC ($59^oS \pm 1^o$). Shading shows uncertainties estimated by a bootstrapping technique. 57

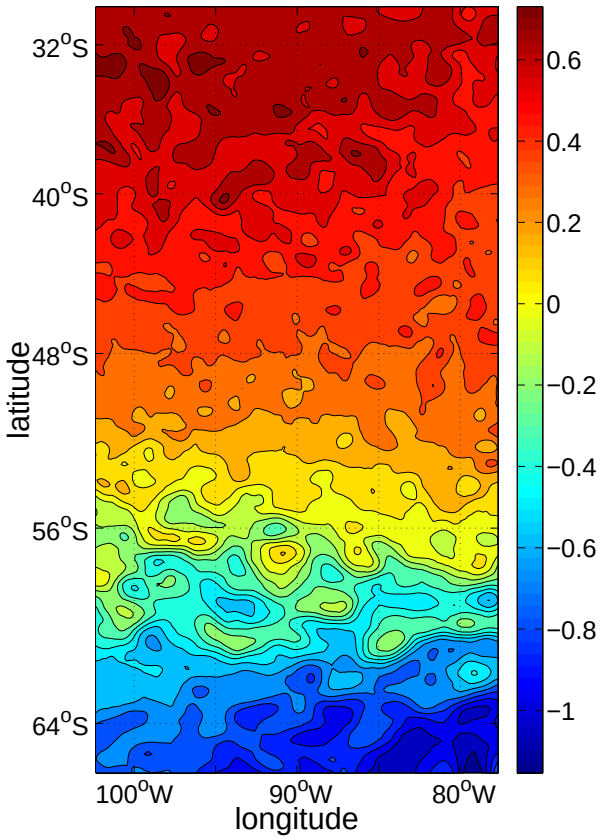

Figure 1: Snapshot of sea surface height [m] as estimated from the combined processing of the TOPEX, ERS-1 and ERS-2 altimetries for an ACC sector upstream of Drake Passage between 103^o-78^oW and 30^o-66^oS.

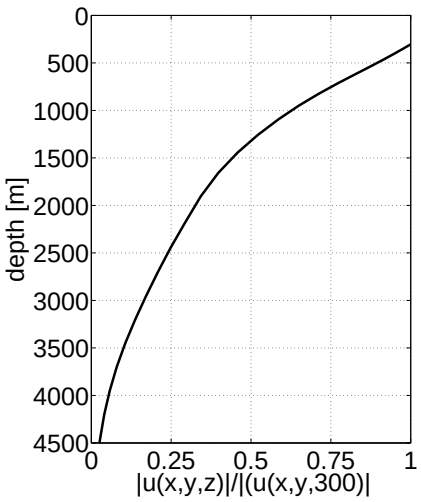

Figure 2: The equivalent-barotopic structure function $\mu(z) = \langle |\boldsymbol{u}(x,y,z)|/|\boldsymbol{u}(x,y,300)| \rangle$ as a function of depth calculated from SOSE. Note that the velocities are scaled relative to 300 m to avoid Ekman fluxes in the mixed layer.

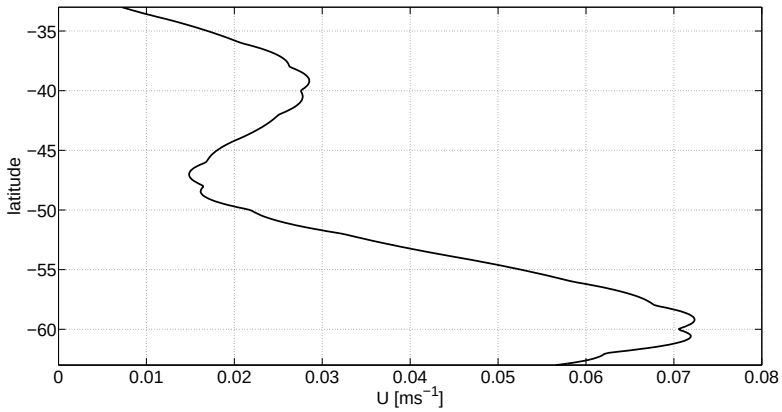

Figure 3: Zonal mean surface velocity for the domain shown in Fig. 1.

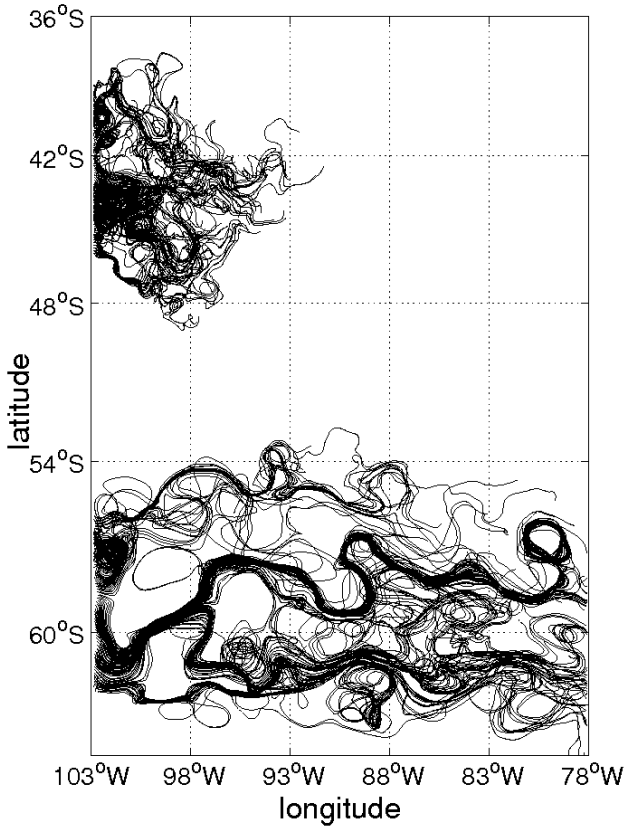

Figure 4: Numerical trajectories for two clusters of approximately 100 particles released between 103^oW-103.5^{o}W and 40^oS-46^{o}S (upper cluster) and 103^oW-103.5^{o}W and 56^oS-62^{o}S (lower cluster). Particle trajectories are shown for the first 150 days. When particles leave at the eastern or western boundary, they are reintroduced from the opposite side for the eddy diffusivity calculations. Particles reentering the domain from the west are not shown here to avoid cluttering the figure.

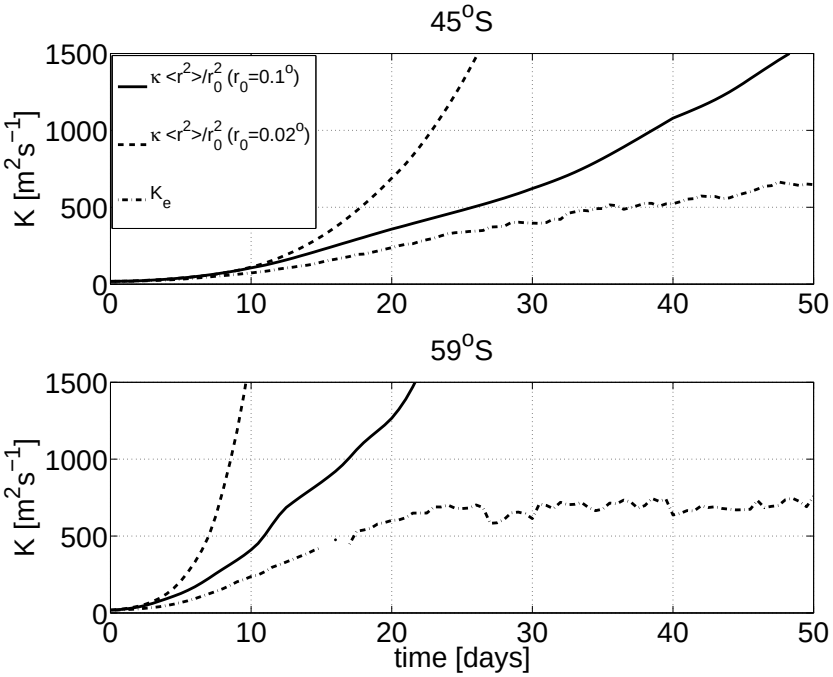

Figure 5: The effective diffusivity K_e defined in Eq. (5) at early times (dottes-dashed lines) compared to the relative dispersion of pairs of particles released along the same latitude line for two different sets of particles, one set released at 0.02^o apart (dashed lines) and the other set released at 0.1^o apart (solid lines). The upper panel is for 45^oS and the lower for 59^oS computed as the equivalent latitude for K_e (see Appendix) and as the latitude at which particles are released.

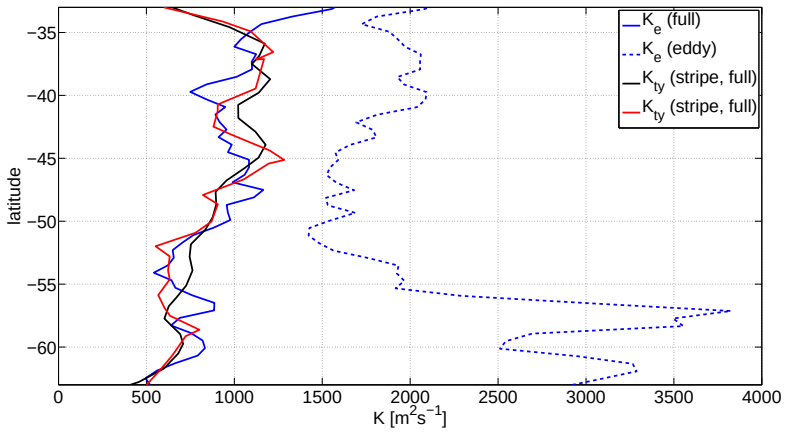

(a)

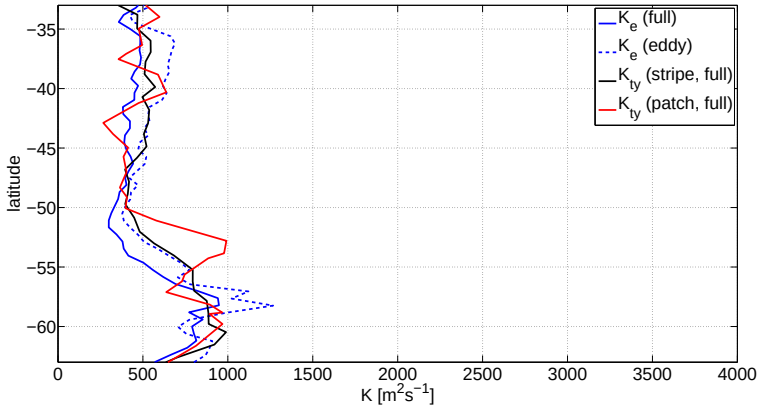

(b)

Figure 6: The effective diffusivity K_e (solid blue lines) defined in Eq. (5), the tracer-based diffusivity K_{ty} defined in Eq. (25) from the spreading of tracer stripes (solid black lines) and tracer patches (solid red lines). Also shown is the effective diffusivity for a tracer advected with the eddy velocity only (dashed blue lines). (a) Diffusivities computed with the surface geostrophic velocity field. (b) Diffusivities calculated with the equivalent-barotropic velocity field rescaled for $\sim 1500\ m$.

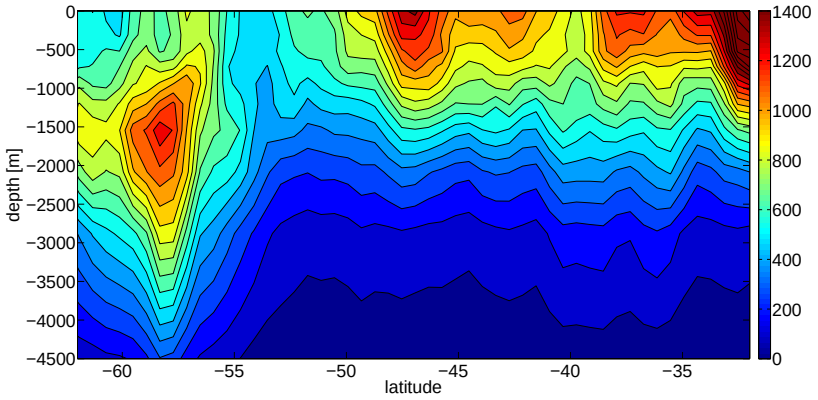

(a)

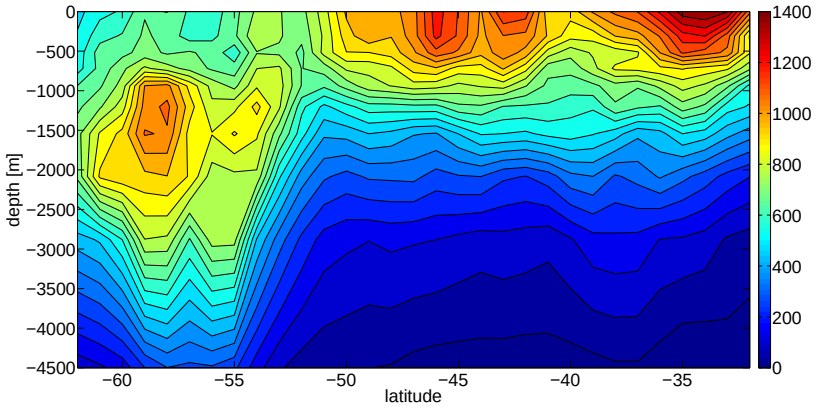

(b)

Figure 7: Latitude-depth maps of (a) the effective diffusivity K_e (Eq. (5)) and (b) the single-particle diffusivity K_{1y} (Eq. (22)) $[m^2 s^{-1}]$. Eddy diffusivities were calculated at 10 depth levels, using the equivalent-barotropic velocity field described in Sec. 3.

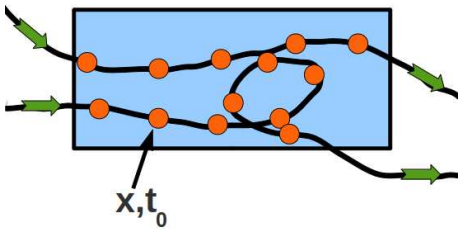

Figure 8: The rectangular box sketches a bin sample used for calculating particle diffusivities from two example trajectories. The orange dots are points at which the trajectory positions are saved. Absolute/relative dispersion are calculated using each of these points as a deployment location, i.e. each of these points is the start of a pseudotrajectory.

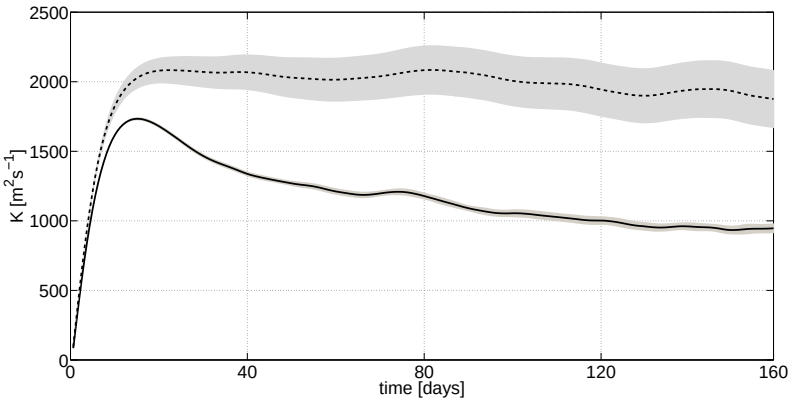

(a)

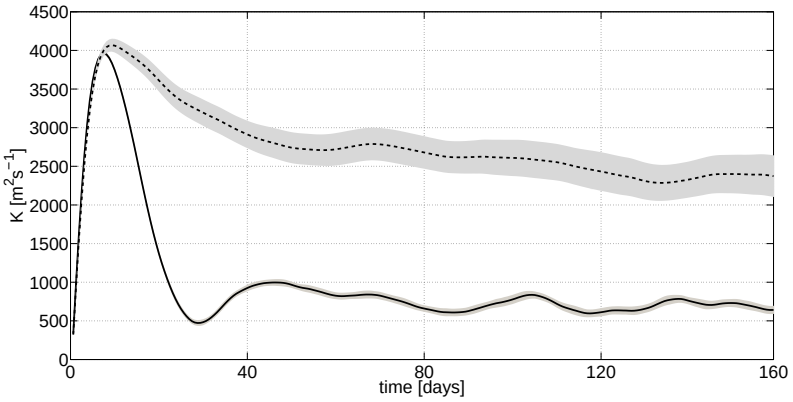

(b)

Figure 9: The single-particle diffusivity, K_{1y} (Eq. (22)) for particles released in 2^o bins in (a) the subtropical gyre ($45^oS \pm 1^o$) and (b) in the ACC ($59^oS \pm 1^o$), both for the full velocity field (solid lines) and for the eddy velocity field (dashed lines). The shaded error bars show 2σ errors estimated by a bootstrapping technique.

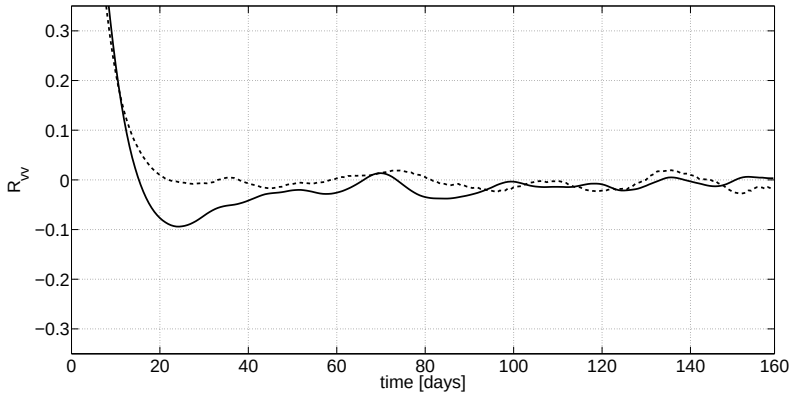

(a)

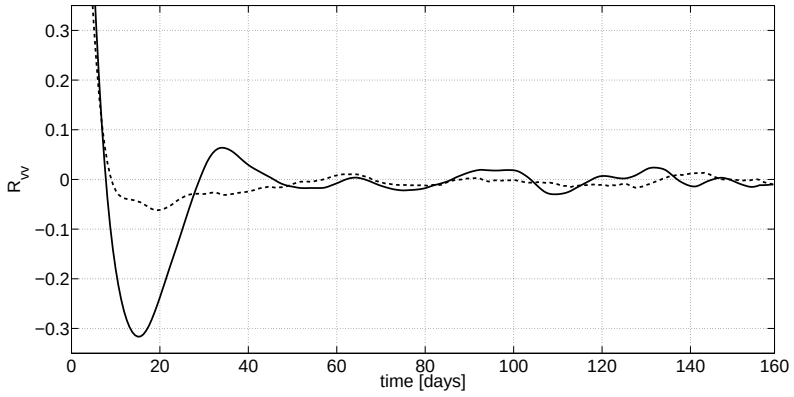

(b)

Figure 10: The Lagrangian velocity autocorrelations, R_{vv}, corresponding to the diffusivities shown in Fig.9, for (a) particles released in a 2^o bin in the subtropical gyre ($45^oS \pm 1^o$) and (b) particles released in a 2^o bin in the ACC ($59^oS \pm 1^o$), both for the full velocity field (solid lines) and the eddy velocity field (dashed lines).

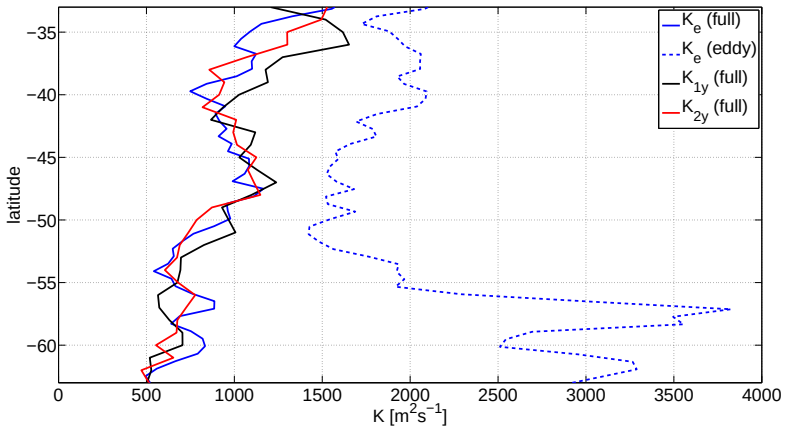

(a)

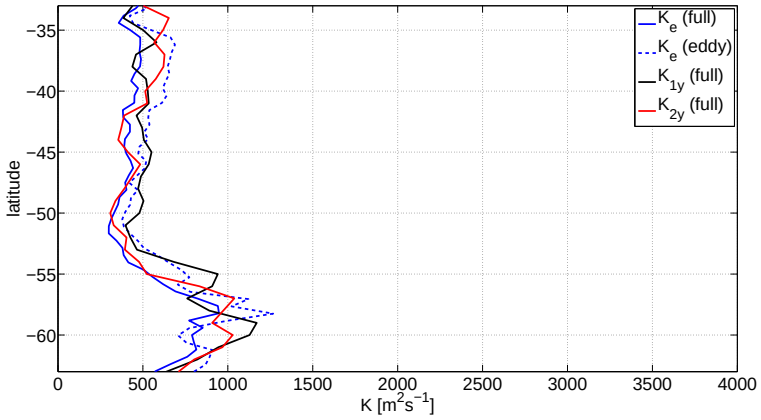

(b)

Figure 11: The effective diffusivity K_e (blue lines) as defined in Eq. (5), the single-particle diffusivity K_{1y} (solid black line) as defined in Eq. (22) and the two-particle diffusivity K_{2y} as defined in Eq. (24) for tracers and particles advected with (a) the surface geostrophic velocity and (b) the velocity at ~ 1500 m, i.e. the surface geostrophic velocity multiplied by 0.4 according to the equivalent-barotropic model for that depth (see Fig. 2). The dashed blue lines are the effective diffusivity K_e for a tracer advected with the eddy velocity only.

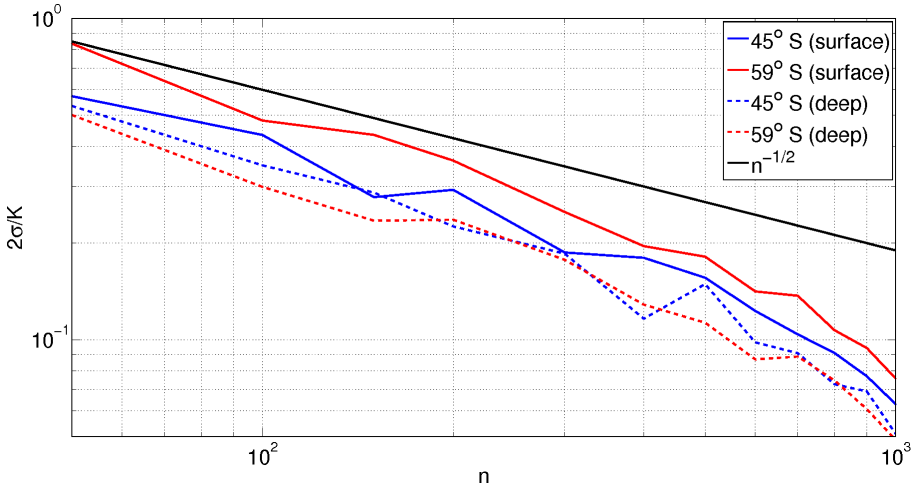

Figure 12: Relative error $2\sigma/K_{1y}$ of the single-particle diffusivity K_{1y} (Eq. (22)), where σ is the standard deviation calculated from bootstrapping with 100 sub-samples of n particles. The errors are shown for particles released in a 2^o bin in the subtropical gyre ($45^oS \pm 1^o$) (blue) and particles released in a 2^o bin in the ACC ($59^oS \pm 1^o$) (red) for the surface (solid lines) and deep surface (dashed lines). The solid black line shows a line with slope of $n^{-1/2}$.

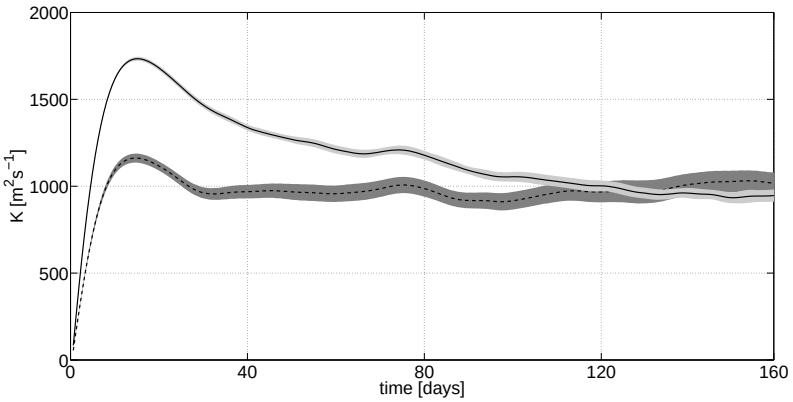

(a)

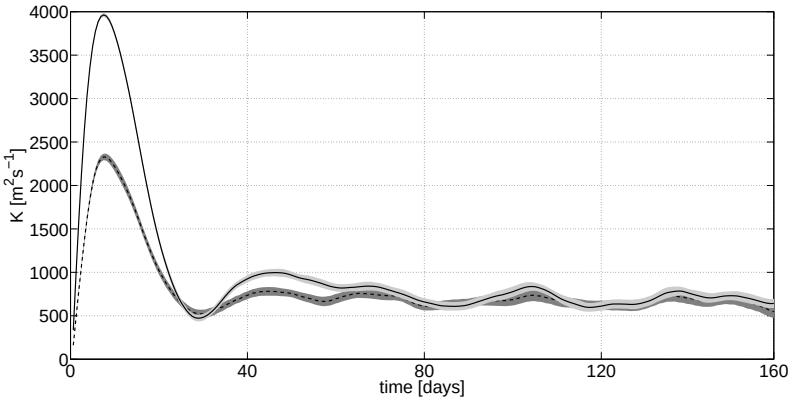

(b)

Figure 13: The time evolution of the single-particle diffusivities K_{1y} (Eq. (22), solid line) and the relative diffusivities K_{2y} (Eq. (24), dashed line) for (a) particles released in a 2^o bin in the subtropical gyre ($45^oS \pm 1^o$) and (b) particles released in a 2^o bin in the ACC ($59^oS \pm 1^o$). Shading shows uncertainties estimated by a bootstrapping technique.

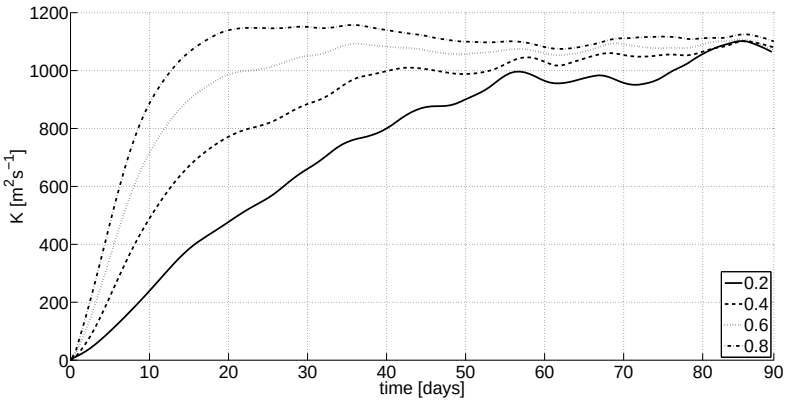

(a)

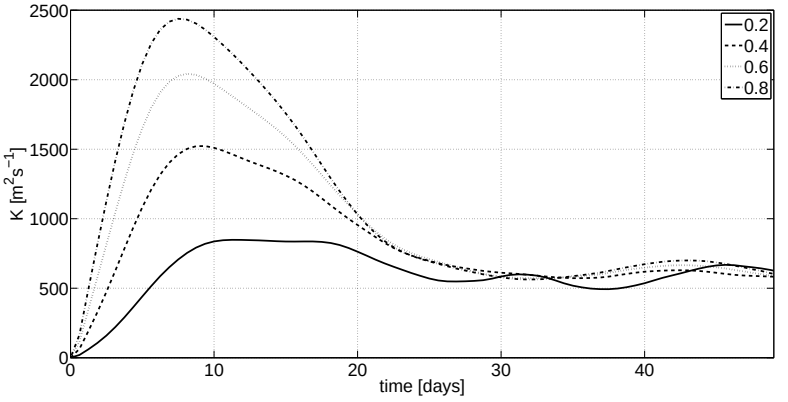

(b)

Figure 14: The time evolution of the two-particle diffusivities K_{2y} (Eq. (24)) for different initial separations for (a) particles released in a 2^o bin in the subtropical gyre ($45^oS \pm 1^o$) and (b) particles released in a 2^o bin in the ACC ($59^oS \pm 1^o$).

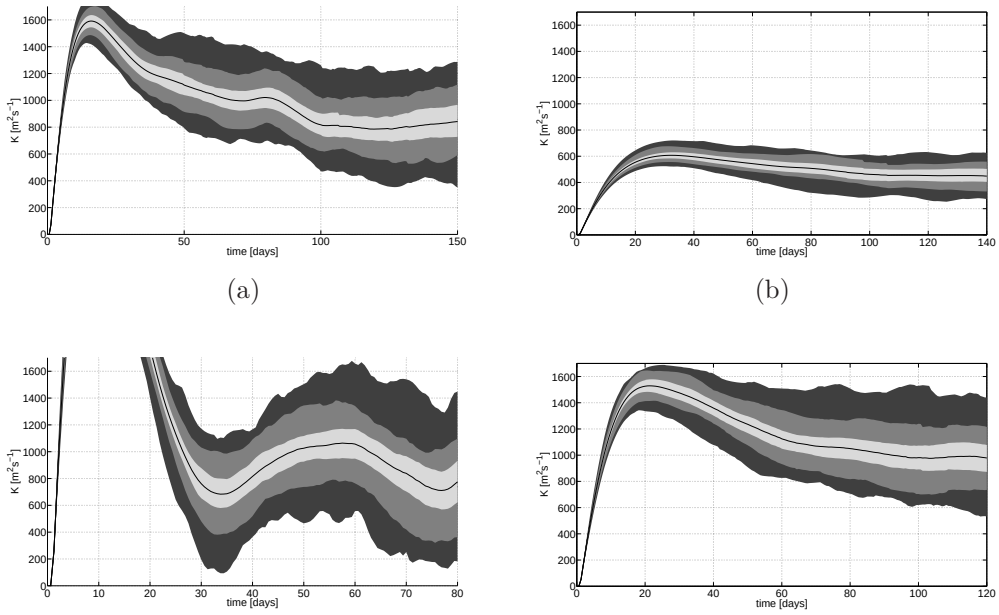

Figure 15: The single-particle diffusivity K_{1y} (Eq. (22)) for particles released in a bin north of the ACC (a) at 500 m and (b) at 1500 m (the bin extends from 44^o to 48^oS) and for particles released in a bin in the ACC (c) at 500 m and (d) at 1500 m (the bin extends from 56^o to 60^oS). Grey shading shows the 5th and 95th percentiles determined by a bootstrapping technique with 100 sub-samples using 50 floats (dark grey), 150 floats (medium grey) and 1000 floats (light grey).